Mechanical behaviour of diamond reinforced metals

Kay A. Weidenmann, R. Tavangar, L. Weber

Angaben zur Veröffentlichung / Publication details:

Weidenmann, Kay A., R. Tavangar, and L. Weber. 2009. "Mechanical behaviour of diamond reinforced metals." *Materials Science and Engineering: A* 523 (1-2): 226–34. https://doi.org/10.1016/j.msea.2009.05.069.

Mechanical behaviour of diamond reinforced metals

K.A. Weidenmann*, R. Tavangar, L. Weber

Ecole Polytechnique Fédérale de Lausanne, EPFL, Laboratory for Mechanical Metallurgy, Station 12, CH-1015 Lausanne, Switzerland

1. Introduction

Metal/diamond composites containing diamonds based on CVD or HPHT synthesis or containing polycrystalline diamonds (PCD) are state-of-the-art materials for the use in drills and grinding tools subjected to high stresses. Grinding wheels for hard metals, diamond tools like cut-off wheels and drills for concrete cutting, tunnelling or oil exploration are typical applications. For these purposes, materials made by powder metallurgy are typically used featuring diamond contents between 10 and 30 vol.%. The bonding between the diamonds and the surrounding matrix material as well as the mechanical properties – above all: the hardness – are of major interest as they predetermine the economic life-time of the tools [1,2].

In contrast, diamond reinforced metals with higher volume contents of embedded diamond particles (>50 vol.%) represent a new class of metal/diamond composites. These composites are promising materials for heat sinks for the cooling of heat-dissipating electronic parts as they offer both excellent thermal conductivity and low thermal expansion. Typical devices to be cooled by using this class of composites are laser diodes or microprocessors in laptops [3–6]. While the thermophysical properties of such composites have been reported in recent contributions [7–9], little information is available about their mechanical behaviour. Such data are however desperately needed to estimate, e.g. warping upon thermal cycling in layered structures such as typical semiconductor–insulator–substrate assemblies.

Beside the practical engineering aspect there is also a fundamental interest in studying the mechanical behaviour of metal matrix composites containing high volume fractions of very strong particles. As it has been shown by Miserez et al. [10], the fracture toughness of aluminium-based MMCs reinforced with high loadings of alumina single crystalline particles increased with particle size up to the point where the particles start breaking. In logical continuation of that work, it would be interesting to see to what point the fracture toughness may be improved if particle fracture can be prevented by using even stronger particles.

In the following we therefore present data on the mechanical behaviour of metal matrix composites containing 55–60 vol.% of diamond particles. As matrix materials we have focussed on pure Al, Cu–2.5 at.% B, and Ag–11 at.% Si, since these are matrix materials used in thermal management due to their high thermal

* Corresponding author at: Universitaet Karlsruhe (TH), Institut fuer Werkstoffkunde I, Kaiserstrasse 12, D-76131 Karlsruhe, Germany. Tel.: +49 721 608 4165; fax: +49 721 608 8044.

E-mail address: kay.weidenmann@iwk1.uka.de (K.A. Weidenmann).

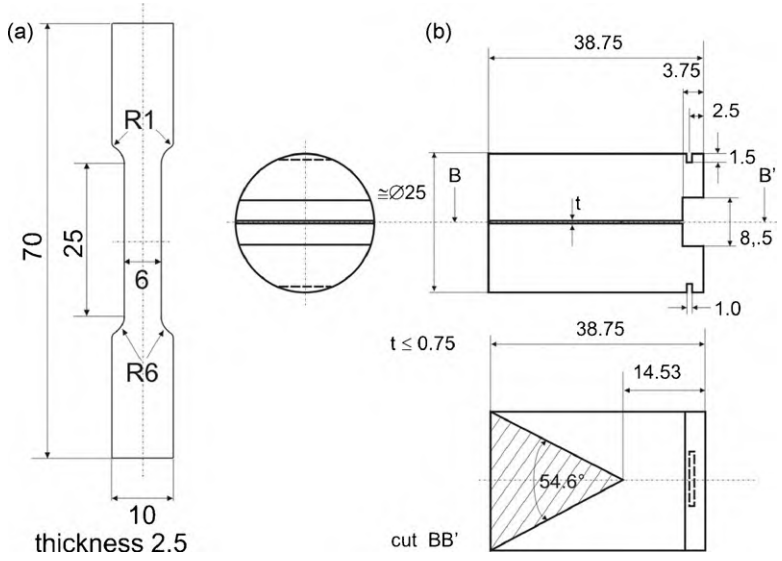

Fig. 1. Specimen geometry for tensile testing (left) and Chevron notch tests according to ASTM E 1304-97 [11].

conductivity, as well as Al–2 wt.% Cu in order to obtain fracture toughness data comparable to those reported by Miserez et al. [10].

2. Experimental

2.1. Materials and processing

The specimens for the tensile tests and the Chevron notch tests according to ASTM E 1304 [11] were manufactured by gas pressure driven infiltration of the chosen pre-alloyed alloys (Al–2 wt.% Cu, Cu–2.5 at.% B, Ag–11 at.% Si) and commercially pure aluminium (Al99.99) into tapped and vibrated powder beds of synthetic diamond with different grit sizes. The synthetic diamond was of the MBD4 quality and purchased from Luoyang High-Tech Qiming Superhard Materials Co. Ltd., China. Tensile specimens were made by infiltration to net shape using stacked graphite plates into which the cavity corresponding to the geometry of the tensile specimen was milled.

The complexity of the Chevron notch specimens' geometry did not allow for getting a net-shape production. The Chevron notch specimens were therefore cut by electro-erosion from infiltrated cylindrical rods of outer diameter corresponding to the size of the Chevron notch short-bar samples. Fig. 1 shows the specimen geometries for both testing procedures.

Table 1 gives an overview of the characterized composite configurations. Chevron notch tests were carried out exclusively on composites with Al–2 wt.% Cu matrix with four different average particle sizes. For the other matrices the investigations focussed on tensile tests of composites featuring the smallest and largest powder particle size investigated. A typical dimension for the powder particle size is the grit mesh size which can be correlated with an average powder particle diameter according to Table 2.

A schematic drawing of the infiltration chamber is shown in Fig. 2. The infiltration cycle consisted in pulling the vacuum very slowly (over several hours) to prevent fluidization of the powder bed. Once a vacuum of roughly 0.01 mbar was reached, heating was started using an induction coil and a graphite susceptor for efficient coupling. The heating rate was approx. 10–20 K min^{-1}. The infiltration temperature for composites with aluminium-based matrices was 1073 and 1373 K for the silver-based and 1410 K for the copper-based compounds. Once the temperature was reached, the system was held at temperature for roughly 30 min to allow equilibration of the temperature. Argon gas was then applied to pressurize the infiltration chamber. The infiltration pressure was adapted to the specimen geometry as well as to the matrix alloy to ensure a proper infiltration of the specimens and chosen such that the threshold pressure for infiltration was exceeded by a factor of at least 3, which leads for quite regularly shaped particles to >99% of filling of the interparticle space [12]. For the tensile specimens the pressure used was 1.5 MPa. For the rods representing a larger powder bed volume to be infiltrated and serving for the production of Chevron notch samples the pressure was increased to 4 MPa. The infiltration was followed by directional solidification that typically should avoid any solidification shrinkage in the composite. During infiltration and solidification the graphite cover plate impeded floating of the diamond powder and consequently a separation of the matrix alloy and the diamonds. After removing from the graphite mould, the specimens were cleaned by sandblasting. Additionally, the Al–2 wt.% Cu matrix composites were subjected to heat treatments. The heat treatment was chosen to be as close as possible to the conditions used by Miserez et al. [10] and consisted of a solutionizing step at 515 °C in air for 10 h and subsequent water-quenching. One chevron notch bar (Al–2 wt.% Cu + MBD4 500/600) was artificially aged at 100 °C for 12 h (heat treatment state T6) while all the rest of the Al–2 wt.% Cu composites were aged at room

Table 1
Examined specimen states.

Grit mesh size (diamond)	Matrix material			
	Al99.99	Al–2 wt.% Cu	Cu–2.5 at.% B	Ag–11 at.% Si
140/170	TT	TT, CN	TT	TT
230/270	–	TT, CN	–	–
325/400	–	TT, CN	–	–
500/600	TT	TT, CN	TT	TT

–: not characterized; TT: tensile tests; CN: Chevron notch tests

Table 2
Correlation between mesh size and average particle diameter for the diamond powders used.

Mesh size	70/80	140/170	230/270	325/400	500/600
Particle diameter (μm) (average value)	200	100	67	40	22

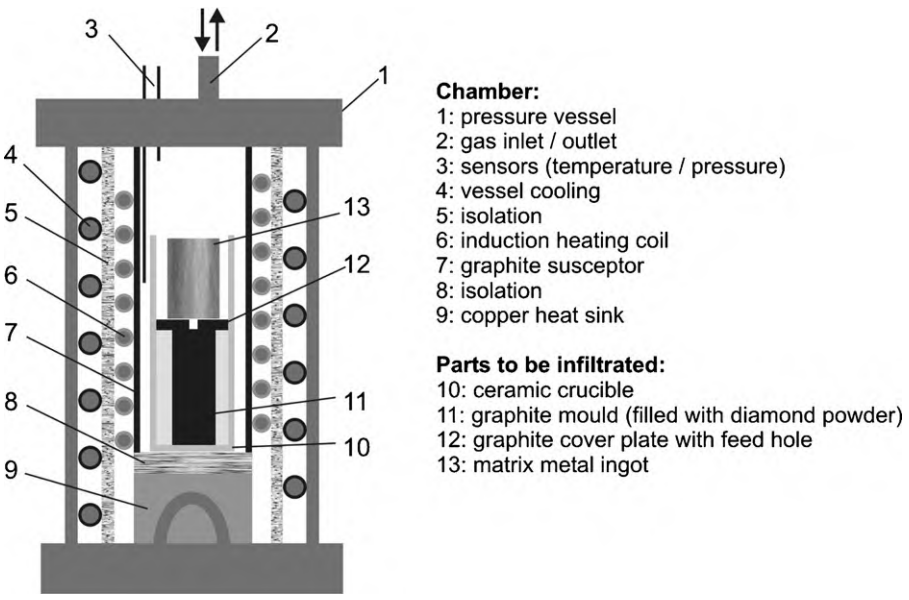

Fig. 2. Schematic drawing of the construction of the infiltration chamber used.

temperature (heat treatment state T4) in order to detect a potential influence of the heat treatment state on the mechanical properties which have been observed to be pronounced for the toughness [10].

2.2. Experimental setup

The tensile tests were carried out on a screw-driven universal testing machine with a maximum load capacity of 10 kN. The strain was measured by inductive extensometers on both sides of the specimen. The tensile tests were displacement controlled at a nominal strain rate of 10^{-3} s^{-1}. After defined total strain increments of 5×10^{-4}, the specimen was repeatedly unloaded to 30% of the previous maximum load and directly reloaded to 70% of that load. This cyclic loading was repeated 8 times before the tensile test was continued. This procedure was repeated until the specimen broke and served to determine the evolution of the specimen's stiffness during quasi-static loading which can be correlated with the damage evolution of the composite [13,14]. During the first four cycles the values for Young's modulus may vary due to the microplasticity in the matrix material and these were therefore disregarded for the evaluation. Further cycling resulted in stabilizing the sample stiffness [13,15]. Consistently, from the first unloading procedure at a total strain of 5×10^{-4} the initial Young's modulus E_0 of the sample was determined. This procedure has recently been applied by the authors to diamond reinforced composites with very high reinforcement contents [16]. The Chevron notch tests according to ASTM Standard [11] were carried out to quantify the toughness of the investigated metal/diamond composites, a method in principle appropriate for brittle materials. The SEM investigations on fractured samples were carried out in a conventional Zeiss EVO 50 SEM. To improve the surface conductivity, the samples were gold sputtered prior to the examination.

3. Results

3.1. Tensile tests

The mechanical behaviour reported in the following corresponds to the average of three tensile specimens for each material. Initial Young's modulus, E_0, of the composites was 300, 250, 240 and 150 GPa for composites with Ag–11 at.% Si, Al–2 wt.% Cu, Al99.99 and Cu–2.5 at.% B as matrix, respectively. The value for the Cu–2.5 at.% B composites was surprisingly low, cf. Fig. 4.

All of the samples exhibited very little plastic deformation to fracture. Therefore only the ultimate tensile strength (UTS) is reported here. The UTS evolved in similar fashion as Young's modulus, the highest value being obtained for the Ag–11 at.% Si matrix as 314 MPa for the small diamond particles and 214 MPa for the large diamond particles, followed by the Al–2 wt.% Cu-based composites reaching roughly 140 MPa, and the pure Al composites with somewhat lower values between 90 and 125 MPa. The Cu-based composites were again exceptionally low featuring a UTS just below 50 MPa. As expected there was no significant effect of particle size on Young's modulus. The UTS on the other hand was for the case of the Ag-based composites considerably higher for the composites containing 22 μm diamonds compared with their counterparts with larger diamond particles. For the pure Al and the Cu–2.5 at.% B-based composites the tendency was inverted and the composites with larger particles had even higher UTS than their finer counterparts. For the Al–2 wt.% Cu-based composites the size influence was much weaker but a slight decrease in strength with increasing particle size was observed. Interestingly enough, plastic strain to failure increased with increasing particle size in the composites with Al–2 wt.% Cu matrix, cf. Fig. 3. Table 4 summarizes the results of the tensile tests for the investigated composite configurations. The effective diamond content of the samples also given in Table 4 was determined from density measurements which were carried out on a conventional analytical balance with a precision of ±10 μg equipped with a special kit to determine the sample density using Archimedes's principle. Subsequently, the diamond volume contents were calculated assuming the volume fraction of porosity and potential interface phases being negligible being aware that these microstructural parameters may have a certain influence. The potential influence of the aluminium carbide interface as well as the porosity especially on the rigidity of the composites has been reported and discussed by the authors recently [16].

The Young's moduli measured by cycling at regular intervals reveal a stiffness drop during the tensile testing for all materials tested. As the composites reinforced with diamonds of the grit mesh size 140/170 tend to have the largest ductility and allow consequently for several measurements, Fig. 4 shows a comparison of representative specimens with such particles embedded in the dif-

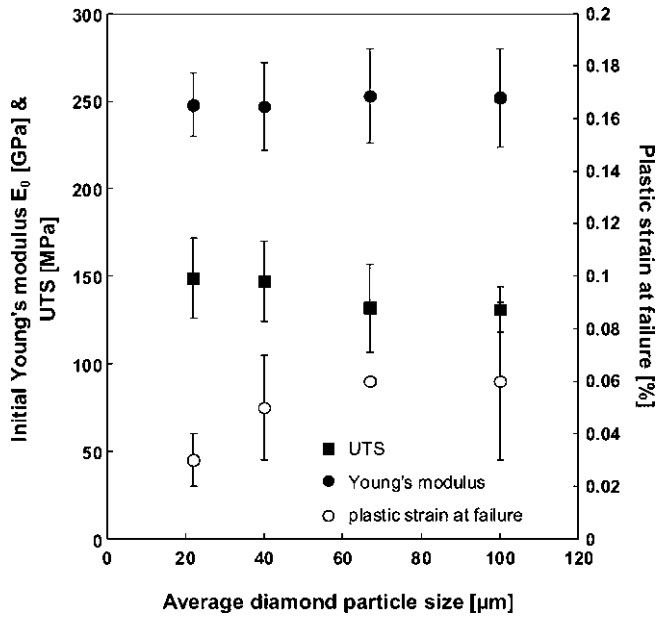

Fig. 3. Correlation between the average diamond particle size and the mechanical properties for Al–2 wt.% Cu matrix composites.

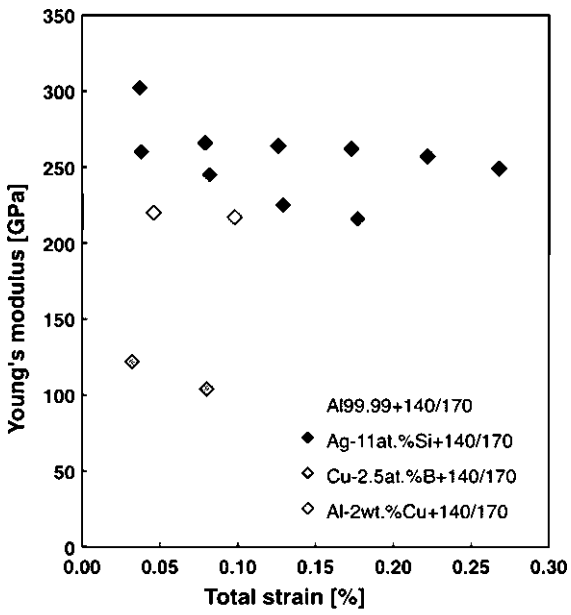

Fig. 5. Evolution of the sample stiffness in terms of change of the Young's modulus at different strain levels for representative specimens reinforced with diamonds of the grit mesh size 140/170.

ferent matrix materials investigated. The stiffness of the samples – always referred to as Young's modulus – was determined from the slope of the unloading steps in engineering stress–strain plots. For cycles that showed hysteresis, the modulus was determined in the linear part of the unloading branch, corresponding to roughly 15–20 data points [16]. The displacement range over which the modulus was measured was on the order of 1–3 μm, whereas the A/D conversion resolution of the LVDT was in on the order of 5 nm and signal noise was on the order of 50–100 nm. The average Young's modulus was calculated from measurements done on three specimens. In the literature [13–15] Young's modulus evolution is usually measured as the slope in true stress, true strain coordinates. Since the true stress–true strain calculation is based on volume conservation, which is not obeyed as long as elastic strains are of the same order than plastic strains and since the total strains are very small, we consider our procedure as good as the one based on true stress and true strain.

Comparing the last determined values for the stiffness with the first one – the initial Young's modulus E_0 – all the specimens show a decrease of 15–18% except the Al–2 wt.% Cu + 140/170 sample. In this case, the stiffness drop is only some GPa as the initial Young's modulus for this sample is already well below the average value of E_0 for the whole batch. In fact, the sample shown is the only one of this batch that allowed for determining the sample stiffness after both 0.05 and 0.1% total strain. However, if the final Young's modulus of this sample is correlated to the average value of the batch, the decrease in stiffness is also about 15%. This is also true for the copper-based composites with an early onset of damage evolution indicated by the low value of E_0. Investigations on the stiffness evolution for specimens reinforced with smaller particles (grit mesh size 500/600 corresponding to 22 μm average size) revealed also a certain decrease, but less pronounced (1–4%).

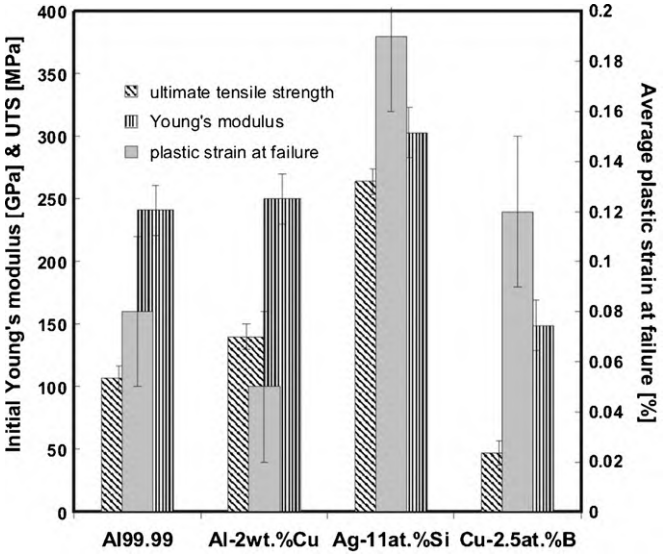

Fig. 4. Average mechanical properties disregarding the diamond particle size for the different matrix materials used.

3.2. Chevron notch fracture toughness tests

The Chevron notch tests were limited to composites having an Al–2 wt.% Cu matrix. Table 4 summarizes the test results as average values for three specimens tested for each specimen type. All investigated specimen types show plasticity factors of 0.21 or higher. These values are well above the limit of 0.1 given by the ASTM standard [11] and the value of 0.2 proposed by Grant et al. [17]. Therefore, calculating the fracture toughness K_{Ic} or K_{Iv} from the determined value K_{Qv} was not possible. Consequently, the toughness value K_{IvM} was calculated from the maximum value in the load–COD curve. The correlation between diamond particle size and the properties determined from the Chevron notch tests is shown in Fig. 6 for the composites in T4 state. As supposed from the results of the tensile tests, the plasticity factor – an indicator for the ductility of the specimens – increases with increasing diamond particle size, while for the toughness values K_{IvM} and K_{Qv} a maximum is observed at an average grain size of 40 μm. As K_{IvM} is determined from the maximum load occurring during the Chevron notch tests, this indicates that at this grain size the test loads also reached a maximum.

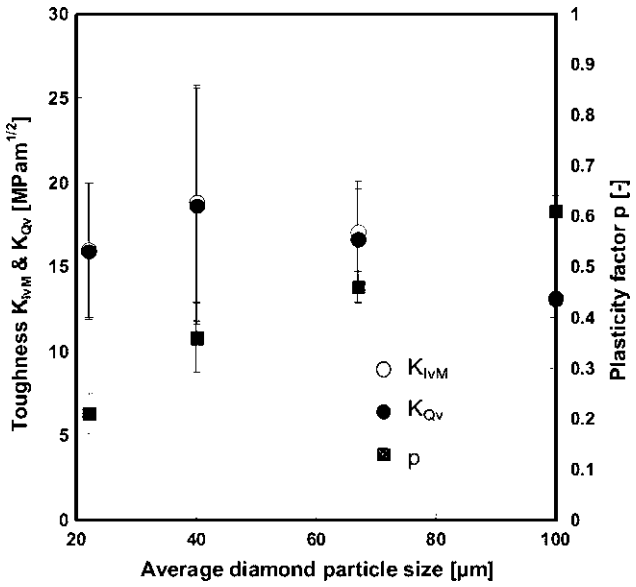

Fig. 6. Correlation between the average diamond particle size and the average mechanical properties determined in chevron notch tests for Al–2 wt-% Cu-matrix composites in heat treatment state T4.

For the heat treatment state T6 the plasticity factor does not change significantly while the toughness values are significantly reduced.

3.3. SEM investigations

No significant influence of the particle size on the mechanical properties for Al–2 wt.% Cu composites could be detected. The SEM micrographs presented below focus, therefore, on the influence of different matrix materials on the microstructure evolution in metal/diamond composites. Figs. 7–10 show fractured surfaces of composites reinforced with diamond particles of the same mesh size (140/170).

The comparison gives evidence that different topographies and interface morphologies occur. In aluminium-based composites both ductile deformed areas in-between the diamond particles and an interfacial phase with a platelet-like structure are observed. It is well-known since 1970s that in aluminium/carbon composites aluminium carbide may occur as interfacial phase [18–20]. For aluminium/diamond composites Ruch et al. [8] have also shown that aluminium carbide (Al_4C_3) is forming. At higher magnifications (cf. Fig. 11) the typical platelet structure also reported by Ruch et al. [8] is clearly visible allowing us to identify the interfacial phase to be aluminium carbide. The composition and microstructure of interfacial phases potentially forming in Al/diamond composites was recently reported by Beffort et al. [21].

In silver-based or copper-based diamond reinforced composites, the diamond surfaces on the fractured specimen surfaces are uncovered. It can be seen that in diamond reinforced Ag–11 at.% Si the matrix material shows ductile behaviour forming a dimple morphology which can be correlated to the relatively high ultimate strain of the material determined from tensile tests. Additionally, matrix material sticking to some diamond surfaces in direct neighbourhood to bare diamond surfaces shows that the crack propagation has not only taken place inside the matrix material but also through the diamond particles. The latter indicates high local stresses in the tensile specimen, in line with the high ultimate tensile strength determined for this composite configuration. Diamond reinforced Cu–2.5 at.% B showing also metal-free diamond particle surfaces obviously fail due to debonding at the diamond/matrix interface. Hence, it is improbable that the bare diamond surfaces indicate fractured diamond particles. The pervasive debonding indicates poor adhesion between copper matrix and diamond leading to severe internal damage of the composite's microstructure at small deformation.

Table 3
Elastic properties of the phases and the effective matrix.

Phase	G (GPa)	K (GPa)	E (GPa)	ν
Cu–2.5 at.% B	48.3	137.8	129.7	0.343
Ag–11 at.% Si	29.6	99.0	80.7	0.357
Al–2 wt.% Cu	26	76	70	0.346
Diamond	478	443	1055	0.103

4. Discussion

4.1. Tensile behaviour

The elastic properties of the composites investigated in this work can be assessed against model predictions. For alumina/aluminium composites of comparable volume fraction of inclusions it has been reported that the generalized self-consistent scheme (GSCS) of Christensen and Lo [22] was in good agreement with the experiment [23]. The experimentally measured rigidity of diamond composites based on Ag–11 at.% Si and Al–2 wt.% Cu matrices with volume fractions of up to 75 vol.% was recently reported by the authors [16] and found to be consistent with predictions based on the differential effective medium (DEM) model [24] at high particle contents. The Cu–2.5 at.% B is assimilated to a pure copper matrix (the 1.5 vol.% boron having a negligible effect on matrix stiffness) while the Ag–11 at.% Si matrix is itself modelled as composites due to the presence of roughly 11 vol.% Si inclusions. For both modelling schemes, i.e. the DEM and the GSC, the effective matrix elastic constants are very close and one single set of elastic constants has been used for the Young's modulus calculation of the Ag–Si/diamond composites. The elastic constants of all matrices are given in Table 3. The values thus predicted for the present composites using both models are given in Table 4 together with the experimental values showing good agreement with experiment, except for the Cu–2.5 at.% B-based composites. For those, the expected values should be roughly 3 times higher than the measured values, indicating that there is a serious problem in the material. As the SEM pictures reveal, the interface between Cu–2.5 at.% B and diamond is very weak as indicated by the ubiquitous separation between particles and matrix. This is at the same time rational for the very low UTS observed for these materials. These results are somewhat contradictory to the results presented by Weber and Tavangar [9] on the thermal properties of Cu–2.5 at.% B/diamond composites. They found that the interface between matrix and diamond at a boron content of 2.5 at.% should be strong as thermal conductivity is high and the composite CTE is low, indicating that the interface is at least strong enough to transmit the stresses required to prevent the copper from free expanding.

We have to admit that further research has to be done to clarify these somewhat contradictory results. Nevertheless, it has to be stated, that the interfacial strength of the composites has not been measured directly. In this contribution, the mechanical properties and the SEM investigations indicate a mechanically weak interface. Weber and Tavangar focussed exclusively on physical properties like thermal conductivity and CTE and found out that the interfacial properties allow for a good heat transfer as well for a low CTE. From this it was deducted, that the interfacial strength should be high. In fact, it could be high enough to result in sufficient thermophysical properties but too low to transfer high mechanical loads resulting in the mechanical properties measured.

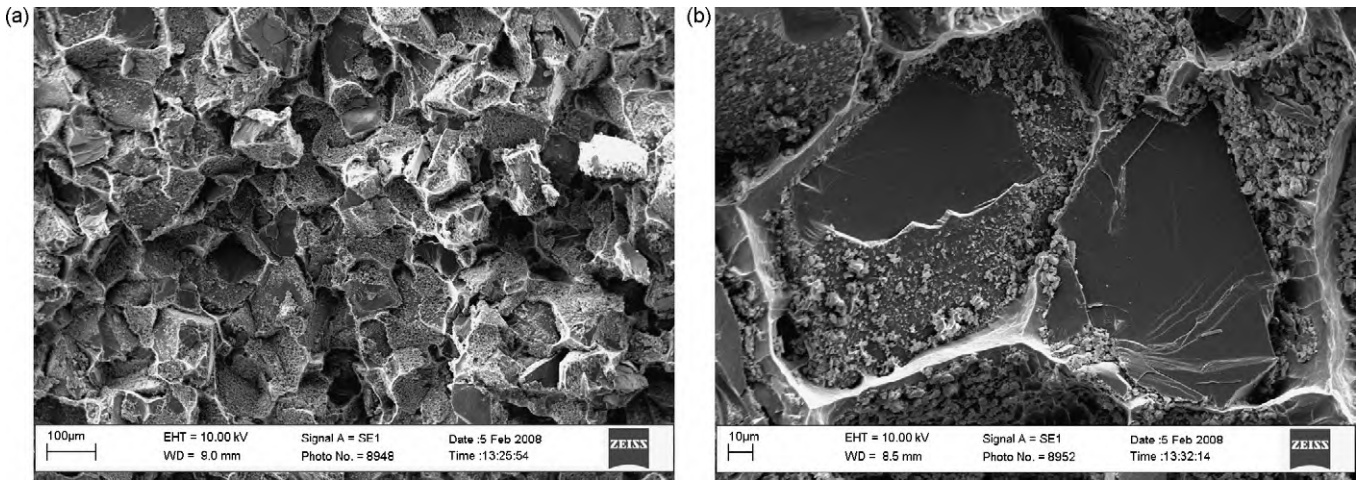

Fig. 7. SEM micrographs of an Al99.99 + 140/170 composite at different magnifications.

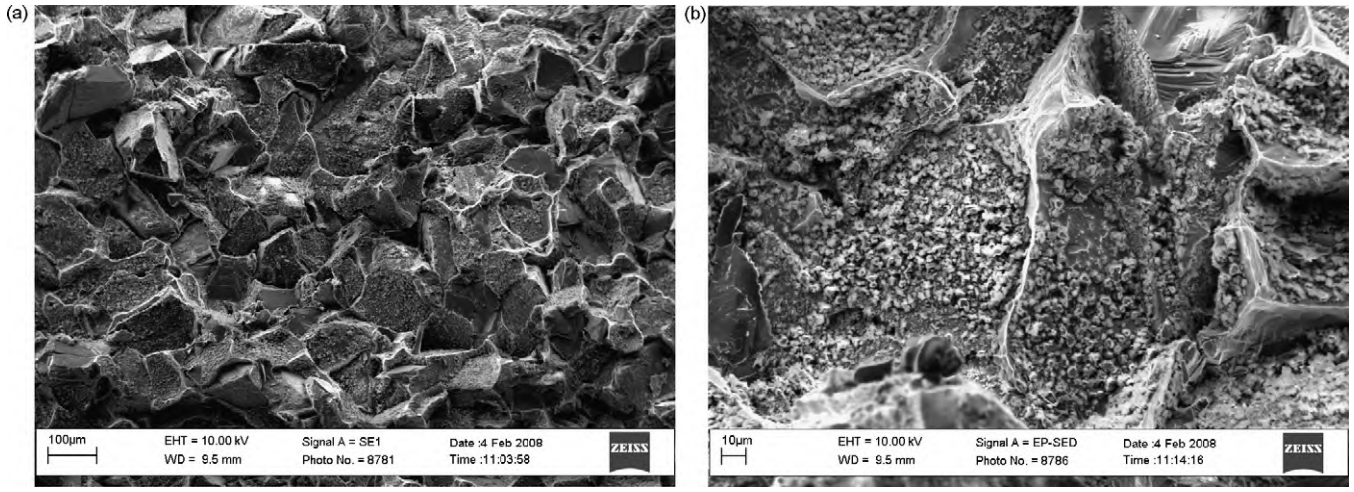

Fig. 8. SEM micrographs of an Al–2 wt-% Cu + 140/170 composite at different magnifications.

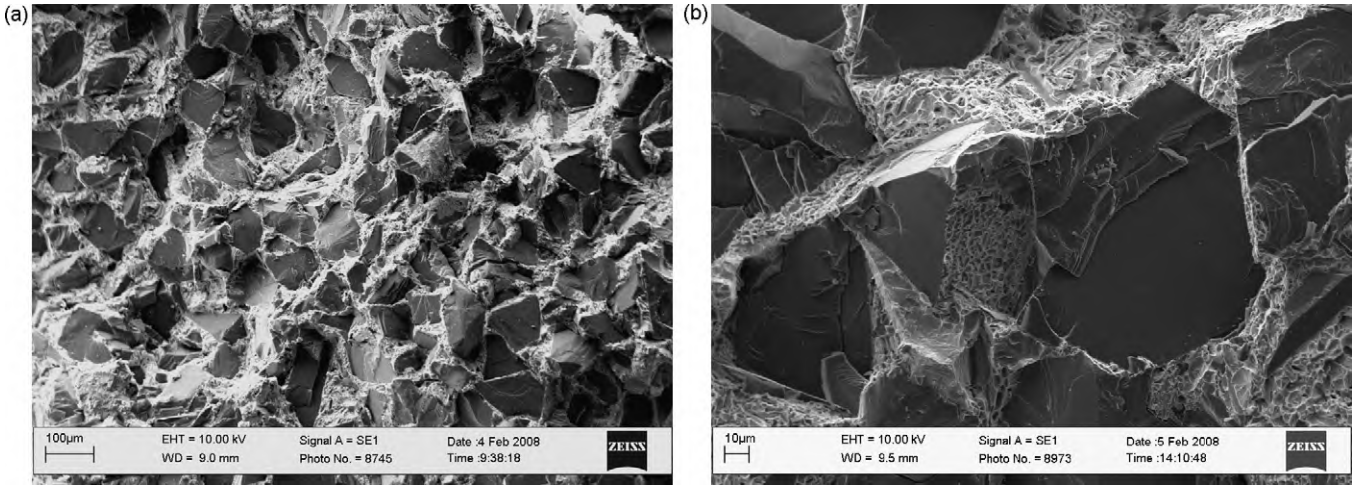

Fig. 9. SEM micrographs of an Ag–11 at-% Si + 140/170 composite at different magnifications.

Additionally, processing factors, for example the infiltration parameters chosen and the constraints imposed by the net-shape mold, could have influenced the interfacial properties in the present case. After cooling down from the infiltration temperature residual stresses evolve in the specimens. This is much more pronounced in the tensile specimens as the specimen geometry and the net-shape graphite mould result in a pre-straining, i.e. a positive residual stress at the interfaces in tensile direction. This effect may also reduce the mechanical properties of the tensile specimens due to an interface failure at early loading stages.

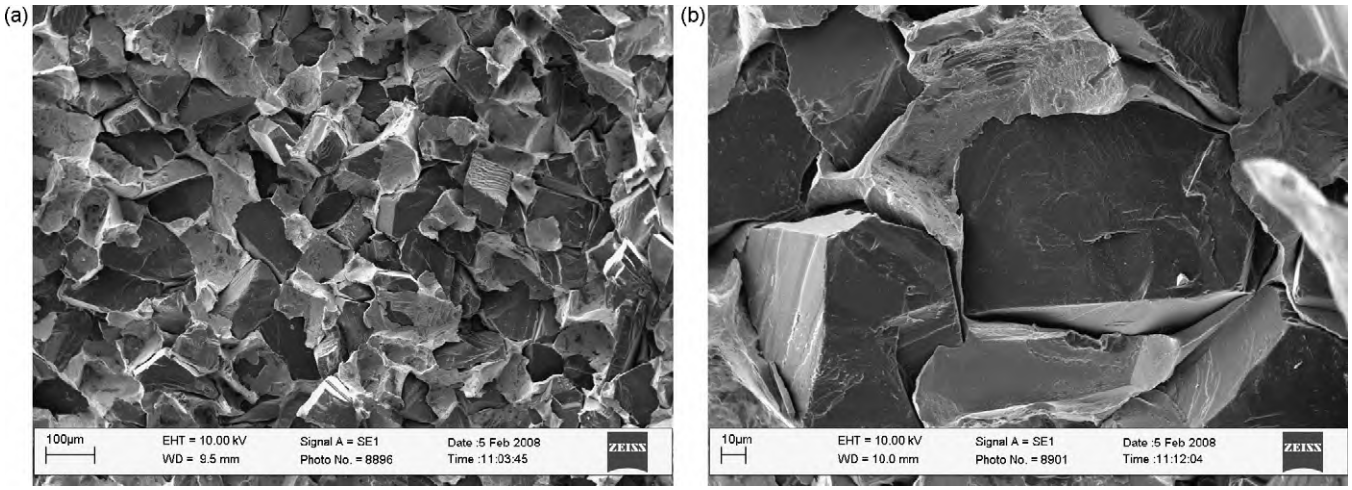

Fig. 10. SEM micrographs of an Cu–2.5 at-% B + 140/170 composite at different magnifications.

The very limited strain to failure observed in metal/diamond composites is in contrast with the much larger strain to failure reported by Kouzeli et al. [13] in alumina/aluminium composites made by the same processing route. For the composites with Cu–2.5 at.% B this can be rationalized by the weak interface, cf. Fig. 10. For the other composites no gap indicating debonding at the interface is visible (cf. Figs. 7–9). From that point, there is no reason why the strain to failure should be so much reduced compared with the Al/alumina case [13] except the fact, that the formation of aluminium carbide can be clearly seen. This phase is well-known to mar the mechanical properties, if occurring in a pronounced manner [19].

At least for the Al–2 wt.% Cu-based composites the evolution of the strain to failure with particle size, cf. Fig. 3, can be used to rationalize the absence of a size effect on the UTS: the composites with larger particles that are expected to be inherently weaker

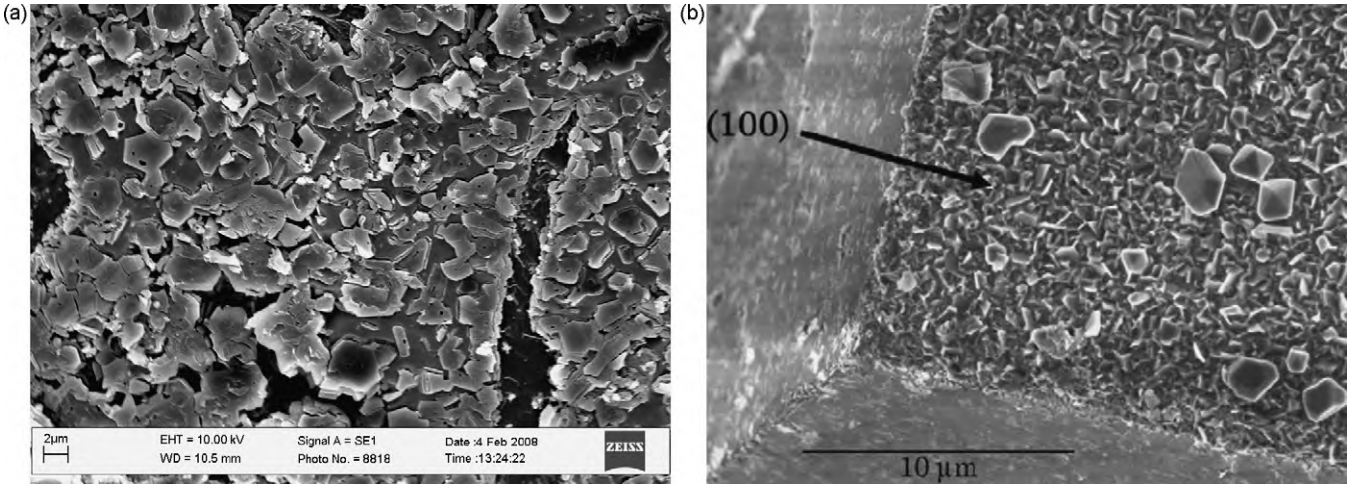

Fig. 11. SEM micrograph (5000×) of the interfacial phase forming in an aluminium/diamond composite (left) in comparison to the aluminium carbide phase found by Ruch et al. [8] (right).

Table 4
Results of the tensile tests on diamond reinforced metals.

Specimen type	Vol frac. diamond	E_0 (GPa)	E_0 (GSCS)[a] (GPa)	E_0 (DEM)[b] (GPa)	UTS (MPa)	Plastic strain at failure (%)
Al99.99 + 500/600	0.54	237 ± 6	218	235	90 ± 2	0.03 ± 0.02
Al99.99 + 140/170	0.54	245 ± 18	218	235	124 ± 11	0.12 ± 0.05
Ag–11 at.% Si + 500/600	0.60	305 ± 1	286	309	314 ± 15	0.19 ± 0.02
Ag–11 at.% Si + 140/170	0.58	301 ± 14	272	292	214 ± 6	0.19 ± 0.03
Cu–2.5 at.% B + 500/600	0.58	162[c]	372	391	44 ± 5	0.12 ± 0.06
Cu–2.5 at.% B + 140/170	0.59	135 ± 11	380	400	49 ± 3	0.11 ± 0.02
Al–2 wt.% Cu + 500/600	0.57	248 ± 18	234	255	149 ± 23	0.03 ± 0.01
Al–2 wt.% Cu + 325/400	0.56	247 ± 25	229	248	137 ± 23	0.05 ± 0.02
Al–2 wt.% Cu + 230/270	0.57	253 ± 27	234	255	132 ± 25	0.06 ± 0.00
Al–2 wt.% Cu + 140/170	0.56	252 ± 28	229	248	131 ± 13	0.06 ± 0.03

[a] Calculated value according to the generalized self-consistent scheme model.
[b] Calculated value according to the differential effective medium model.
[c] Due to the low strength of the specimens only one valid value for E_0 could be determined.

Table 5
Results of the Chevron notch tests on diamond reinforced metals.

Specimen type	K_{IvM} (MPa$\sqrt{m}$)	p	K_{Qv} (MPa$\sqrt{m}$)	Min. Ø B^a (mm)	Corr. Eq. (2) (MPa$\sqrt{m}$)
Al–2 wt.% Cu + 500/600 T4	16.0 ± 4	0.21 ± 0.04	15.9 ± 4	14.2	19.7 ± 4
Al–2 wt.% Cu + 325/400 T4	18.8 ± 7	0.36 ± 0.07	18.6 ± 7	23.0	27.1 ± 8
Al–2 wt.% Cu + 230/270 T4	17.0 ± 3	0.46 ± 0.03	16.6 ± 3	19.8	27.3 ± 5
Al–2 wt.% Cu + 140/170 T4	13.2 ± 6	0.61 ± 0.03	13.1 ± 6	12.5	26.6 ± 11
Al–2 wt.% Cu + 500/600 T6	9.9 ± 2	0.26 ± 0.06	10.9 ± 1	8.8	14.2 ± 2

[a] The diameter of the samples was 25 mm.

due to a lower dislocation density [25] compensate this effect by a somewhat higher strain to failure which leads to a roughly constant ultimate tensile strength. On the other hand, for the Ag–11 at.% Si-based composites where the plastic strain to failure is no longer small compared with the elastic strain just before rupture, the expected size effect could be observed: the composite with 22 μm average particle size was 50% stronger than the composite reinforced with particles of 100 μm average size.

A key to the limited strain to failure may be found in the strong decrease of Young's modulus in the diamond composites investigated here, cf. Fig. 5. While the overall decline of Young's modulus from the level of E_0 to the last modulus value measured in unloading–loading cycles prior to rupture is 15–18% (for the large particles) and a few percent for the small particles, and thus intriguingly close to the one observed in Al/alumina composites [13,25], it happens over a much smaller strain, indicating that damage is accumulating much faster in the present composites than in their Al/alumina counterparts. Kouzeli et al. [25] have developed a simple model to estimate the strain to failure, ε_f, from the damaging rate:

$$\varepsilon_f = \frac{n}{1 - ((d\ln(E/E_0))/d\varepsilon)} \quad (1)$$

with n being the strain hardening exponent of the matrix. Applying this model to the present case, we take from Fig. 4 that $d\ln(E/E_0)/d\varepsilon$ takes values of roughly −100 in the diamond composites (18% over 0.2% of strain). Therefore, with a strain hardening exponent between 0.1 and 0.2 the expected strain to failure would indeed be on the order of 0.1–0.2% which is in reasonable agreement with experiment. However, the question why Young's modulus drops so rapidly in the present composites cannot be answered at this point.

4.2. Fracture toughness

The fracture toughness evaluated by the maximum load on Chevron notch short rod specimen shows a maximum for the particles of 40 μm nominal average size. At the same time the plasticity factor p increases with increasing particle size and is in all cases above the value of 0.1 accepted by the ASTM standard and even above the less conservative limit of 0.2 suggested by Grant et al. [17].

The maximum toughness is thus at somewhat larger particle sizes than obtained for the Al/alumina case by Miserez [10,26], i.e. between 10 and 35 μm for angular (i.e. irregularly shaped) particles and 25 μm for polygonal (i.e. regularly shaped) alumina single crystals. The absolute values of fracture toughness K_{IvM} of the present composite are for the solution treated and naturally aged (T4) Al–2 wt.% Cu matrices on the same order of magnitude as for the angular alumina particles investigated by Miserez [10,26], while the polygonal alumina single crystalline particles yielded composites with significantly larger fracture toughness. On the other hand, the plasticity factors in the experiments by Miserez [10,26] were in general much smaller. A large plasticity factor p observed in the Chevron notch test indicates large irreversible energy consumption upon crack propagation. This can be either due to large scale plastic deformation or due to energy dissipation by damage mechanisms in the wake of the crack tip. The former should be detected by violation of the minimum size criterion. As can be seen in Table 5 this was not the case for any of the materials tested as all samples comply with the size criterion given by the standard. Therefore, we consider the energy being consumed by damage in the wake of the crack tip. Since that energy is actually used to propagate the crack, one may use the correction for non-zero p suggested by Barker [27]. The K_{Ic} may then be estimated by:

$$K_{Ic} \approx K_Q \left(\frac{1+p}{1-p}\right)^{1/2} \quad (2)$$

Applying this correction to our experimental data it can be seen that the maximum in K_{IvM} with regard to particle size is not maintained in the equivalent K_{Ic} data: instead, the fracture toughness becomes a virtually stable value for particle sizes above 40 μm, cf. Table 5. However, the validity of this correction, Eq. (2), has only been experimentally verified up to $p = 0.25$ and the justification of this extension to higher p-values would require experimental assessment of our materials by alternative methods, e.g. the J-integral test.

5. Conclusions

Diamond reinforced metals feature very high Young's moduli i.e. 3–4 times greater than those of the unreinforced matrix materials. Good strength in tension ranging from roughly 100 MPa for composites based on pure aluminium to 300 MPa for composites with an Ag–11 at.% Si matrix was achieved. However, the mechanical performance is strongly dependent on the load transfer between the diamond particles and the matrix. This is exemplified by Cu–2.5 at.% B-based composites with roughly 60 vol.% of diamond, for which the interface is weak and both Young's modulus and fracture strength are very low, i.e. 145 GPa and 50 MPa, respectively. For Ag–11 at.% Si and aluminium-based composites fracturing of the diamond particles was observed which could be either (a) due to excellent interfacial bonding by a well-balanced aluminium carbide content or (b) due to a pronounced carbide formation degrading the mechanical properties of the diamond particles in a way that fracture of the particles occur. Though the aspect of aluminium carbide formation in Al/diamond composites has been recently investigated [8,21], the influence on the mechanical properties of the diamonds or the interface, respectively, should be looked at in detail in future. In general, for all composites investigated, the ductility is very low and limits their use for structural applications.

Acknowledgement

The research project on which this paper is based is kindly supported by a scholarship of the German Research Foundation (DFG) under the Contract No. WE 4273/1-1 for one of the authors (K.A. Weidenmann).

References

[1] S.W. Webb, Diam. Relat. Mater. 8 (1999) 2043–2052.
[2] X. Xu, X. Tie, H. Wu, Int. J. Refract. Met. Hard Mater. 25 (2007) 244–249.

[3] C. Zweben, J. Met. 44 (7) (1992) 15–23.
[4] C. Zweben, J. Met. 50 (6) (1998) 47–51.
[5] C. Zweben, Adv. Mater. Proc. 163 (12) (2005) 33–37.
[6] K. Yoshida, H. Morigami, Microelectron. Reliab. 44 (2004) 303–308.
[7] J.-M. Molina, M. Rhême, J. Carron, L. Weber, Scripta Mater. 58 (2008) 393–396.
[8] P.W. Ruch, O. Beffort, S. Kleiner, L. Weber, P.J. Uggowitzer, Comp. Sci. Technol. 66 (2006) 2677–2685.
[9] L. Weber, R. Tavangar, Scripta Mater. 57 (2007) 988–991.
[10] A. Miserez, S. Stücklin, A. Rossoll, C. San Marchi, A. Mortensen, Mater. Sci. Technol. 18 (11) (2002) 1461–1470.
[11] ASTM Standard E 1304-97, Annual Book of ASTM Standards, 1997.
[12] M. Bahraini, J.-M. Molina, M. Kida, L. Weber, J. Narciso, A. Mortensen, Curr. Opin. Sol. State Mater. Sci. 9 (2005) 196–201.
[13] M. Kouzeli, L. Weber, C. San Marchi, A. Mortensen, Acta Mater. 49 (2000) 497–505.
[14] R. Tavangar, S. Nategh, L. Weber, Mater. Sci. Technol. 20 (2004) 1645–1648.
[15] P.B. Prangnell, T. Downes, P.J. Withers, W.M. Stobbs, Acta Met. Mater. 42 (1994) 3437–3442.
[16] K.A. Weidenmann, R. Tavangar, L. Weber, Comp. Sci. Technol., in press.
[17] T.J. Grant, L. Weber, A. Mortensen, Eng. Frac. Mech. 67 (2000) 263–276.
[18] M.F. Amateau, J. Mater. Comp. 10 (1976) 279–296.
[19] K.I. Portnoi, N.I. Timofeeva, A.A. Zabolotskil, V.N. Sakovich, B.F. Trefilov, M.Kh. Levinskaya, N.N. Polyak, Soviet Powder Metall. Metal Ceram. 20 (2) (1981) 116–119.
[20] M. de Sanctis, S. Pelletier, Y. Bienvenu, M. Guigon, Carbon 32 (5) (1994) 925–930.
[21] O. Beffort, F.A. Khalid, L. Weber, P. Ruch, U.E. Klotz, S. Meier, S. Kleiner, Diam. Relat. Mater. 15 (2006) 1250–1260.
[22] R.M. Christensen, K.H. Lo, J. Mech. Phys. Solids 27 (1979) 315–330.
[23] M. Kouzeli, Tensile behaviour of aluminium reinforced with ceramic particles, Doctoral Thesis no. 2348, EPFL, Lausanne, Switzerland, 2001.
[24] A.N. Norris, A.J. Callegari, P. Sheng, J. Mech. Phys. Solids 33 (6) (1985) 525–543.
[25] M. Kouzeli, L. Weber, C. San Marchi, A. Mortensen, Acta Mater. 49 (2001) 3699–3709.
[26] A. Miserez, Doctoral Thesis no. 2703, EPFL, Lausanne, Switzerland, 2002.
[27] L.M. Barker, Int. J. Frac. 15 (6) (1979) 515–536.